Circular Cylindrical Absorbing Terminations

Stéphane R. Legault
Thomas B.A. Senior

Radiation Laboratory
Department of Electrical Engineering and Computer Science
The University of Michigan
Ann Arbor, MI 48109-2122

December 15, 1995

1 Introduction

The need to terminate the computational domain used in various numerical methods such as finite elements (FEM) has lead to the development of a number of absorbing boundary conditions (ABCs) as well as various material absorbers [1-4]. Most of this work was done in the context of a planar geometry and it is not immediately apparent how well the performance observed for planar boundaries translates to more general curvilinear ones. Indeed, while it has been shown that it is possible to obtain a perfectly reflectionless interface in the planar case by using a particular anisotropic material [4], it remains to be seen if this is also true for a curvilinear boundary. We therefore examine herein the performance of ABCs as well as material absorbers applied to a circular cylindrical (from now on referred to simply as cylindrical) boundary. The absorption of cylindrical wave functions is first examined at the interface of the various truncation schemes, and expressions for the modal reflection coefficients are obtained. The results are then used to solve for the scattered field due to a perfect electrical conducting (pec) cylinder surrounded by a given absorbing termination.

2 Absorption of Cylindrical Wave Functions

Consider the surface $\rho = \rho_1$ where ρ, ϕ, z are cylindrical polar coordinates, with the surface illuminated by a field from within. The geometry is illustrated in Figure 1. The most general

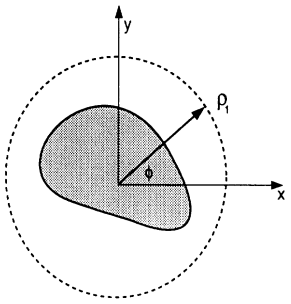

Figure 1: Geometry used to study absorption of cylindrical wave functions

such field can be written as

$$U = \sum_{m=-\infty}^{\infty} a_m H_m^{(2)}(k_0\rho)e^{-jm\phi} \tag{1}$$

originating from sources or a scattering body in $\rho < \rho_1$, and we seek a termination at $\rho = \rho_1$ that will completely absorb the field. The terminations considered are ABCs ranging from first to fourth order, various material interfaces, as well as metal-backed versions of these materials.

2.1 Absorbing Boundary Conditions

The simplest approach to mathematically terminate a computational domain is to impose an ABC at $\rho = \rho_1$. From the corresponding impedance boundary conditions derived using Rytov's [5] method, or, alternatively, from the asymptotic expansion of the Hankel function for large argument (see [1], for example), the following ABCs are found:

$$L_l U = 0 \tag{2}$$

where the first order ($l = 1$) operator is

$$L_1 = \frac{\partial}{\partial\rho} + jk_0 + \frac{1}{2\rho}. \tag{3}$$

A poorer version of this valid for large $k_0\rho$ is

$$L_1' = \frac{\partial}{\partial\rho} + jk_0. \tag{4}$$

The higher second order ABC has

$$L_2 = \frac{\partial}{\partial\rho} + jk_0 + \frac{1}{2\rho} + \frac{j}{2k_0}\left(1 - \frac{1}{jk_0\rho}\right)\left(\frac{1}{\rho^2}\frac{\partial^2}{\partial\phi^2} + \frac{1}{4}\right), \tag{5}$$

and to a lower order (annihilation wise) we have

$$L_2' = \frac{\partial}{\partial\rho} + jk_0 + \frac{1}{2\rho} + \frac{j}{2k_0}\left(\frac{1}{\rho^2}\frac{\partial^2}{\partial\phi^2} + \frac{1}{4}\right). \tag{6}$$

We note that (3),(4),(5) and (6) correspond respectively to zeroth, first, second and third order Rytov approximations. For the fourth order ABC we have

$$\begin{aligned} L_4 \;=\; & \frac{\partial}{\partial\rho} + jk_0 + \frac{1}{2\rho} + \frac{j}{2k_0}\left\{1 - \frac{1}{jk_0\rho} - \right. \\ & \left. \frac{1}{4(k_0\rho)^2}\left[\frac{\partial^2}{\partial\phi^2} + \frac{25}{4} - \frac{4}{jk_0\rho}\left(\frac{\partial^2}{\partial\phi^2} + \frac{13}{4}\right)\right]\right\}\left(\frac{1}{\rho^2}\frac{\partial^2}{\partial\phi^2} + \frac{1}{4}\right). \end{aligned} \tag{7}$$

The extent to which these boundary conditions annihilate the field (1) has been examined by Senior et al [6]. It is found that for small m with $k_0\rho \gg 1$ all of the conditions are reasonably effective, with the amount of suppression increasing with the order of the condition. As m approaches $k_0\rho$, however, the effectiveness decreases, and for $m > k_0\rho$ there is almost no suppression. This is consistent with the fact that the ABCs can be derived from the asymptotic expansion of $H_m^{(2)}(k_0\rho)$ for fixed m and large $k_0\rho > m$. Fortunately, for most fields U the dominant contribution to the infinite series (1) is provided by the terms with $|m| < k_0\rho$, and for $|m| > k_0\rho$ the terms are relatively small. As evident from a Watson transformation applied to the series, and in the context of the planar case, increasing m corresponds to increasing the angle of incidence ϕ on the interface, with $m \simeq k_0\rho$ equivalent to grazing incidence. Alternatively, one may observe that $H_m^{(2)}(x)$ behaves as a traveling wave for $m \ll x$ and as an evanescent wave for $m \gg x$. Such an interpretation supports the fact that the ABCs absorb traveling waves well, but perform more poorly in the case of evanescent waves, in agreement with results obtained for planar interfaces.

For the incident field

$$U^i = H_m^{(2)}(k_0\rho)e^{-jm\phi} \tag{8}$$

the reflected field is

$$U^r = R(m)H_m^{(1)}(k_0\rho)e^{-jm\phi}, \tag{9}$$

and in the case of the ABC given in (2), $R(m) = R_l(m)$ with

$$R_l(m) = -\frac{L_l\{H_m^{(2)}(k_0\rho)e^{-jm\phi}\}}{L_l\{H_m^{(1)}(k_0\rho)e^{-jm\phi}\}}. \tag{10}$$

For fixed m and large $k_0\rho > m$ it can be shown that

$$R_1(m) = O\{(k_0\rho)^{-2}\}, \;\; R_2(m) = O\{(k_0\rho)^{-4}\}, \;\; R_4(m) = O\{(k_0\rho)^{-6}\}, \tag{11}$$

and in contrast to the planar case, none of the $R_l(0)$ is precisely zero. In Figure 2 the reflection coefficients are plotted vs m for $l = 1, 2, 4$ and $k_0\rho = 10 + k_0\lambda_0/2$, and the similarity to the planar counterparts is evident. It must also be pointed out that the reflection coefficients

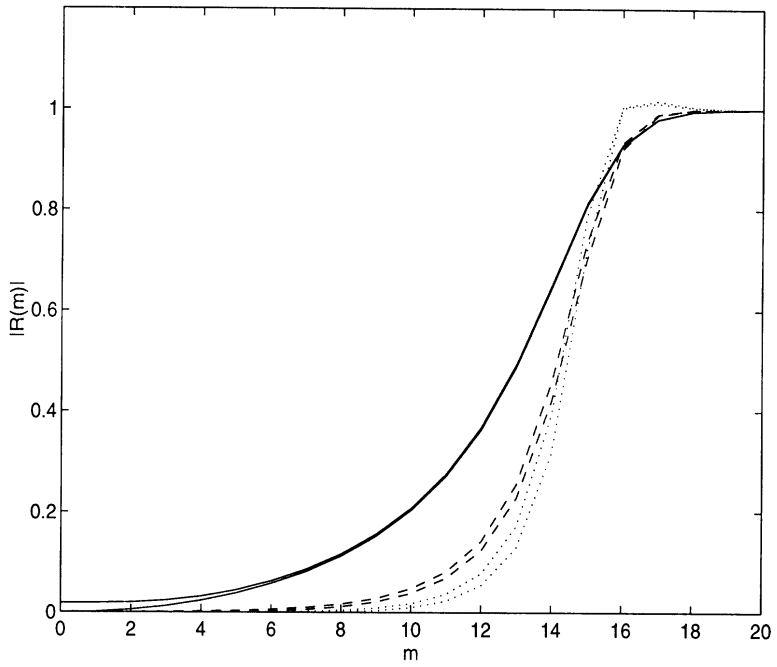

Figure 2: Modal reflection coefficient for ABCs at $x_1 = 10 + \pi$: (——) 1^{st} order ABCs, (– –) 2^{nd} order ABCs and $(\cdots)$ 4^{th} order ABCs. The poorer versions are also given.

for the higher order ABCs actually overshoot unity for $m \simeq 16$. This effect is reminiscent of Gibbs' phenomenon and is accentuated with diminishing x_1. The overshoot disappears as x_1 increases as we tend towards the planar case, and $|R(m)|$ becomes increasingly similar (albeit on a different scale) to the planar reflection coefficient $|R(\phi)|$.

2.2 Material Interfaces

We examine next the implementation of truncation schemes by using various material interfaces. Although an interface alone does not constitute a practical termination scheme, the effectiveness of a metal-backed layer depends on our ability to eliminate (or at least minimize) the interface reflection, and we therefore consider the interface problem first. To this end, it is assumed that the region $\rho \geq \rho_1$ is occupied by a certain material extending out to infinity. As it will ultimately be necessary to terminate the medium at (say) $\rho = \rho_2$ with, for example, a pec, the media examined will all be lossy. The material types studied are homogeneous isotropic and anisotropic materials, as well as inhomogeneous anisotropic ones.

2.2.1 Homogeneous Isotropic Medium

Consider the case when the outer region $\rho \geq \rho_1$ is occupied by a homogeneous isotropic dielectric with $\epsilon_r = \mu_r$. For the incident field (8), the reflection coefficient at the interface

$\rho = \rho_1$ is

$$R(m) = -\frac{H_m^{(2)'}(x) - \Gamma H_m^{(2)}(x)}{H_m^{(1)'}(x) - \Gamma H_m^{(1)}(x)} \tag{12}$$

with

$$\Gamma = \frac{H_m^{(2)'}(\epsilon_r x)}{H_m^{(2)}(\epsilon_r x)} \tag{13}$$

and $x = k_0\rho_1$. From the asymptotic expansions of the Hankel functions for fixed m and large $x > m$,

$$\Gamma = -j\left\{1 + \frac{1}{2j\epsilon_r x} - \frac{4m^2-1}{8\epsilon_r^2 x^2}\left(1 - \frac{1}{j\epsilon_r x}\right) + O(x^{-4})\right\} \tag{14}$$

giving

$$R(m) = -\frac{j}{4x}\left(1 - \frac{1}{\epsilon_r}\right)e^{-2j(x - m\pi/2 - \pi/4)}\left\{1 + +O(x^{-1})\right\} \tag{15}$$

which is small if $x \gg 1$ or if $\epsilon_r \simeq 1$. Note that if we let $|\epsilon_r| \to \infty$, then $\Gamma \to -j$ and the behavior of a lower first order ABC is recovered. This also holds for a planar interface with a homogeneous isotropic medium. Figure 3 gives a plot of $|R(m)|$ for various values of ϵ_r. Given the previously made observations, it is not surprising to see that the behavior is slightly poorer than the first order ABC given in (3). As is the case for the ABCs, good absorption is observed when $m < x$, with total reflection occurring for the evanescent modes when $m > x$.

2.2.2 Homogeneous Anisotropic Medium

For a planar interface, the uniaxial medium proposed by Sacks et al [4] produces a perfect match for all angles of incidence, and represents a substantial improvement over an isotropic medium. We now seek the analog for cylindrical coordinates and assume

$$\bar{\bar{\epsilon}}_r = \bar{\bar{\mu}}_r = a\hat{\rho}\hat{\rho} + b\hat{\phi}\hat{\phi} + c\hat{z}\hat{z} \tag{16}$$

where a, b, c are constants. If the field in the medium is

$$H_z = f(x)e^{-jm\phi} \tag{17}$$

where $x = k_0\rho$ and the ϕ dependence is chosen to match (8), then

$$E_\phi = \frac{jZ_0}{b}\frac{\partial f}{\partial x}e^{-jm\phi} \tag{18}$$

and $f(x)$ satisfies

$$\frac{1}{x}\frac{\partial}{\partial x}\left(\frac{x}{b}\frac{\partial f}{\partial x}\right) + \left(c - \frac{m^2}{ax^2}\right)f = 0. \tag{19}$$

The appropriate solution of this is

$$f(x) = H_\nu^{(2)}(x\sqrt{bc}) \tag{20}$$

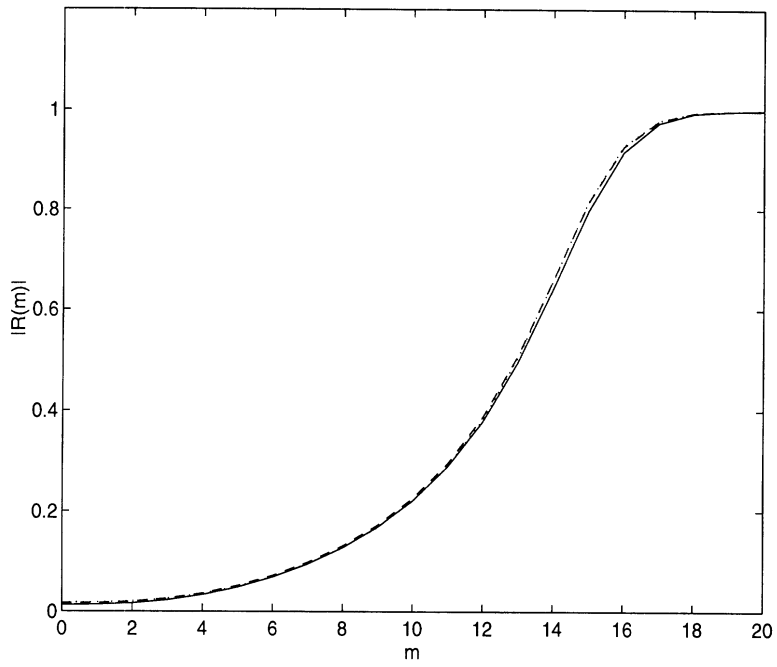

Figure 3: Modal reflection coefficient for homogeneous isotropic interface at $x_1 = 10 + \pi$: (——) $\epsilon_r = 1 - j1$, (— —) $\epsilon_r = 1 - j2$, and $(\cdots)$ $\epsilon_r = 1 - j3$.

with

$$\Gamma = \frac{1}{bf}\frac{\partial f}{\partial x} = \sqrt{\frac{c}{b}}\frac{H_\nu^{(2)'}(x\sqrt{bc})}{H_\nu^{(2)}(x\sqrt{bc})} \tag{21}$$

where $\rho = \rho_1$ and $\nu = m\sqrt{b/a}$. To minimize $R(m)$ for large x, choose $1/a = c = b$ as in the case of a planar surface. Then

$$\Gamma = \frac{H_{mb}^{(2)'}(xb)}{H_{mb}^{(2)}(xb)} \tag{22}$$

with b complex to produce attenuation, and for large $x > m$ we have

$$R(m) = -\frac{j}{4x}\left(1 - \frac{1}{b}\right)e^{-2j(x - m\pi/2 - \pi/4)}\left(1 + O(x^{-1})\right). \tag{23}$$

Compared with the isotropic material, some of the higher order terms in the braces are eliminated, but overall the performance is no better. Nevertheless, as seen in Figure 4, the homogeneous anisotropic material provides some improvement over the isotropic one up to $m \simeq 13$, where the reflection coefficient behaves quite peculiarly. This erratic behavior is apparently attributable to phase reversals of the Hankel function of the second kind with complex order and argument. For a given complex order ν, it can be shown that as $|z|$ increases the function $H_\nu^{(2)}(z)$ behaves as an *incoming wave* for small $|z|$, switching to the typical outgoing wave when $Re(\nu) \simeq Re(z)$. For fixed x and varying m, $H_{mb}^{(2)}(bx)$ is initially

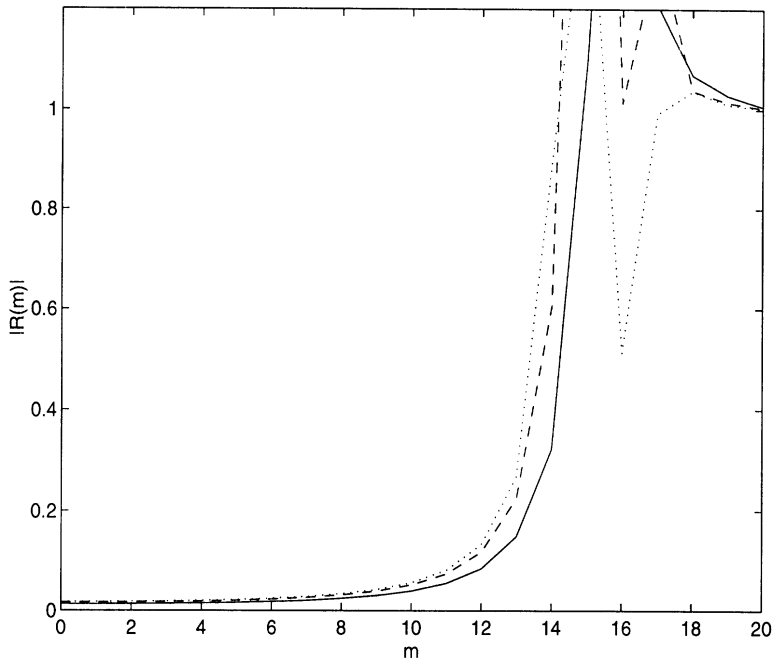

Figure 4: Modal reflection coefficient for a homogeneous anisotropic medium at $x_1 = 10 + \pi$: (——) $b = 1 - j$, (— —) $b = 1 - j2$, and $(\cdots)$ $b = 1 - j3$

outgoing for low values of m but the sharp overshoots above unity indicate values of m where $H^{(2)}_{mb}(bx)$ is incoming instead of outgoing. It will be shown in Section 3 that good results can be obtained nevertheless, at least when considering scattering from a pec cylinder. Comparing $|R(m)|$ for the homogeneous isotropic and anisotropic materials as $m \to 0$ reveals that they behave almost identically. This parallels the case of normal incidence for the planar interface since $m = 0$ is the order of the mode which is normally incident on the cylindrical boundary. The relatively poor performance of the layer (compared to the planar case) is disappointing, since a perfectly matched interface is not achieved. In an attempt to improve the absorption, we next consider an inhomogeneous anisotropic material interface.

2.2.3 Inhomogeneous Anisotropic Medium

We now allow the quantities a, b and c in (16) to be functions of $x = k_0\rho$. Consider the field (17) with

$$f(x) = H^{(2)}_{mb_0}(b_0 y) \tag{24}$$

where b_0 is a constant and $y = \gamma(x)$. Since $f(x)$ must satisfy

$$\frac{1}{y}\frac{\partial}{\partial y}\left(\frac{y}{b_0}\frac{\partial f}{\partial y}\right) + \left(b_0 - \frac{m^2 b_0}{y^2}\right) f = 0 \tag{25}$$

and

$$\frac{\partial f}{\partial x} = \gamma'(x)\frac{\partial f}{\partial y} \tag{26}$$

we have

$$\frac{1}{\gamma(x)\gamma'(x)}\frac{\partial}{\partial x}\left(\frac{\gamma(x)}{b_0\gamma'(x)}\frac{\partial f}{\partial x}\right)+\left(b_0-\frac{m^2 b_0}{\gamma^2(x)}\right)f=0 \tag{27}$$

in agreement with (19) if

$$\begin{aligned} b(x) &= b_0 x\frac{\gamma'(x)}{\gamma(x)} \\ c(x) &= b_0\frac{\gamma(x)\gamma'(x)}{x} \\ a(x) &= \frac{1}{b_0 x}\frac{\gamma(x)}{\gamma'(x)} \end{aligned} \tag{28}$$

Thus

$$a(x)=\frac{1}{b(x)},\quad c(x)=\left(\frac{\gamma(x)}{x}\right)^2 b(x) \tag{29}$$

with $b(x)$ given in (28). Then

$$\Gamma=\frac{1}{bf}\frac{\partial f}{\partial x}=\frac{b_0}{b}\gamma'(x)\frac{H_{mb_0}^{(2)\,\prime}(b_0\gamma)}{H_{mb_0}^{(2)}(b_0\gamma)} \tag{30}$$

so that

$$\Gamma=\frac{\gamma(x)}{x}\frac{H_{mb_0}^{(2)\,\prime}(b_0\gamma)}{H_{mb_0}^{(2)}(b_0\gamma)}. \tag{31}$$

For large $|b_0\gamma|>m$

$$\frac{H_{mb_0}^{(2)\,\prime}(b_0\gamma)}{H_{mb_0}^{(2)}(b_0\gamma)}=-j\left\{1+\frac{1}{2jb_0\gamma}-\frac{4m^2-1/b_0^2}{8\gamma^2}\left(1-\frac{1}{jb_0\gamma}\right)+O\{(b_0\gamma)^{-4}\}\right\}. \tag{32}$$

Hence

$$\Gamma=-j\left\{\frac{\gamma}{x}+\frac{1}{2jb_0 x}-\frac{4m^2-1/b_0^2}{8x\gamma}\left(1-\frac{1}{jb_0\gamma}\right)+\cdots\right\} \tag{33}$$

and therefore

$$R(m)=\frac{j}{2}\Delta e^{-2j(x-m\pi/2-\pi/4)}\left\{1+O(x^{-1})\right\} \tag{34}$$

where

$$\Delta=\frac{H_m^{(2)\prime}(x)}{H_m^{(2)}(x)}-\Gamma. \tag{35}$$

If $\gamma=x$ the medium is again isotropic, and since

$$\Delta=-\frac{1}{2x}\left(1-\frac{1}{b_0}\right), \tag{36}$$

we recover the reflection coefficient (23). Alternatively, if

$$\gamma(x) = x\left(1 + \frac{\alpha_1}{x}\right) \tag{37}$$

with

$$\alpha_1 = \frac{1}{2j}\left(1 - \frac{1}{b_0}\right), \tag{38}$$

then

$$\Delta = -\frac{j}{8x^2}\left(1 - \frac{1}{b_0^2}\right)\left\{1 + O(x^{-1})\right\} \tag{39}$$

giving

$$R(m) = \frac{1}{16x^2}\left(1 - \frac{1}{b_0^2}\right)e^{-2j(x - m\pi/2 - \pi/4)}\left\{1 + O(x^{-1})\right\}, \tag{40}$$

and as judged by the order in x, the performance is now that of the first order ABC (3). More accurately still, if

$$\gamma(x) = x\left(1 + \frac{\alpha_1}{x} + \frac{\alpha_2}{x^2}\right) \tag{41}$$

with α_1 given in (38) and

$$\alpha_2 = \frac{1}{8}\left(1 - \frac{1}{b_0^2}\right), \tag{42}$$

then

$$\Delta = -\frac{1}{16x^3}\left\{4m^2\left(1 - \frac{1}{b_0}\right) - 2 + \frac{1}{b_0^2}\left(1 + \frac{1}{b_0}\right)\right\} \tag{43}$$

giving

$$R(m) = -\frac{j}{32x^3}\left\{4m^2\left(1 - \frac{1}{b_0}\right) - 2 + \frac{1}{b_0^2}\left(1 + \frac{1}{b_0}\right)\right\}e^{-2j(x - m\pi/2 - \pi/4)}\left\{1 + O(x^{-1})\right\}, \tag{44}$$

and the performance is now that of the poorer second order ABC (6).

Unfortunately, it is not possible to continue further in this manner. To reproduce the best second order ABC (5), and thereby come close to a perfectly matched interface, would require

$$\gamma(x) = x\left(1 + \frac{\alpha_1}{x} + \frac{\alpha_2}{x^2} + \frac{\alpha_3}{x^3}\right) \tag{45}$$

with

$$\alpha_3 = \frac{1}{16j}\left\{4m^2\left(1 - \frac{1}{b_0}\right) - 2 + \frac{1}{b_0^2}\left(1 + \frac{1}{b_0}\right)\right\}, \tag{46}$$

and this is unacceptable since it implies a medium whose properties depend on m. However, it does show that the profile of the inhomogeneous medium can be specified to absorb to a higher degree a particular mode by fixing m.

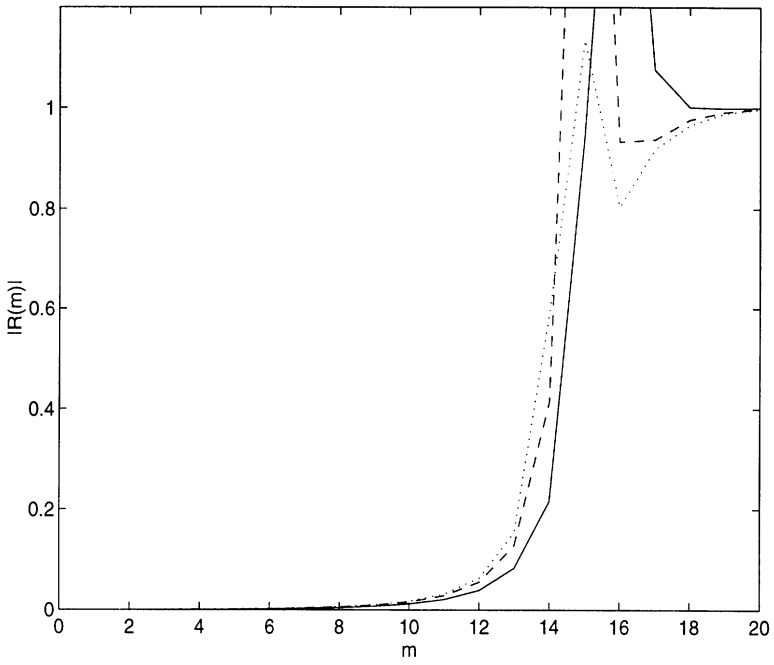

Figure 5: Modal reflection coefficient for a inhomogeneous anisotropic medium at $x_1 = 10 + \pi$: (——) $b = 1 - j$, (— —) $b = 1 - j2$, and $(\cdots)$ $b = 1 - j3$.

Thus, it appears that the nearest counterpart in cylindrical coordinates to a planar perfectly matched layer is the inhomogeneous anisotropic medium (16) with a, b and c given by (28) and (29) and

$$\gamma(x) = x\left\{1 + \frac{1}{2jx}\left(1 - \frac{1}{b_0}\right) + \frac{1}{8x^2}\left(1 - \frac{1}{b_0^2}\right)\right\} \tag{47}$$

where $x = k_0\rho_1$ and b_0 is an arbitrary complex quantity. As indicated by the reflection coefficient (44), the match is significantly superior to that provided by a homogeneous medium for any finite x, but as $x \to \infty$

$$c(x), b(x) \to b_0, \quad a(x) \to 1/b_0$$

as in the planar case. The reflection coefficient $|R(m)|$, using (31) and (47), is plotted as function of m for $x_1 = 10 + k_0\lambda_0/2$ and a sequence of b_0 in Figure 5. The increased absorption for all modes having $m < 13$ is quite pronounced. Note that the oscillatory behavior of $|R(m)|$ is still observed and is explained in the same manner as in the previous section.

2.3 Absorbing Material Layers

Keeping in mind that our objective is to efficiently terminate a given computational domain, we now examine the performance of metal-backed layered versions of the materials presented

above. The geometry is basically as shown in Figure 1, except that we now have a pec located at $x = x_2 = k_0\rho_2 = k_0(\rho_1 + \tau)$. The result is a metal-backed layer of absorbing material of thickness τ located at x_1. Naturally, the behavior as b_0 varies differs from the case of the infinite medium. For example, letting $b_0 \to 1$ leads to $|R(m)| \to 1$ as the layer becomes more transparent. An actual FEM implementation of such a geometry requires a finite value of b_0, and we select here values which are typical of those used in the planar case with similar thicknesses. That is, for a thickness of $\tau = 0.15\lambda_0$, we select an imaginary component in the range of 2 to 3.

2.3.1 Homogeneous Isotropic Layer

It is a straightforward task to show that the reflection coefficient for a metal-backed layer of homogeneous isotropic material with $\epsilon_r = \mu_r = b_0$ is

$$R(m) = -\frac{N_m H_m^{(2)}(x_1) - M_m H_m^{(1)}(x_1)}{N_m H_m^{(2)'}(x_1) - M_m H_m^{(1)'}(x_1)}, \tag{48}$$

where

$$M_m = H_m^{(2)}(b_0 x_1) + \Gamma H_m^{(1)}(b_0 x_1), \tag{49}$$

$$N_m = H_m^{(2)'}(b_0 x_1) + \Gamma H_m^{(1)'}(b_0 x_1), \tag{50}$$

and

$$\Gamma = -\frac{H_m^{(2)'}(b_0 x_2)}{H_m^{(1)'}(b_0 x_2)}. \tag{51}$$

We observe that as $x_2 \to \infty$ then $\Gamma \to 0$ and the solution for the infinite medium is recovered. As for the infinite medium we also recover the behavior of the lower first order ABC as $|b| \to \infty$. Figure 6 illustrates $|R(m)|$ for various b_0 when $x_1 = 10 + k_0\lambda_0/2$ and $x_2 = x_1 + k_0 0.15\lambda_0$. The distinction between the infinite medium and the layer progressively disappears as either τ or b_0 increases, in which case both layered and infinite versions of the medium tend to behave as the first order ABC given in (3).

2.3.2 Homogeneous Anisotropic Layer

The analogous solution for a homogeneous anisotropic layer as presented in Section 2.2.2 may be written in the form (48) with

$$M_m = H_{b_0 m}^{(2)}(b_0 x_1) + \Gamma H_{b_0 m}^{(1)}(b_0 x_1), \tag{52}$$

$$N_m = H_{b_0 m}^{(2)\,\prime}(b_0 x_1) + \Gamma H_{b_0 m}^{(1)\,\prime}(b_0 x_1), \tag{53}$$

and

$$\Gamma = -\frac{H_{b_0 m}^{(2)\,\prime}(b_0 x_2)}{H_{b_0 m}^{(1)\,\prime}(b_0 x_2)}. \tag{54}$$

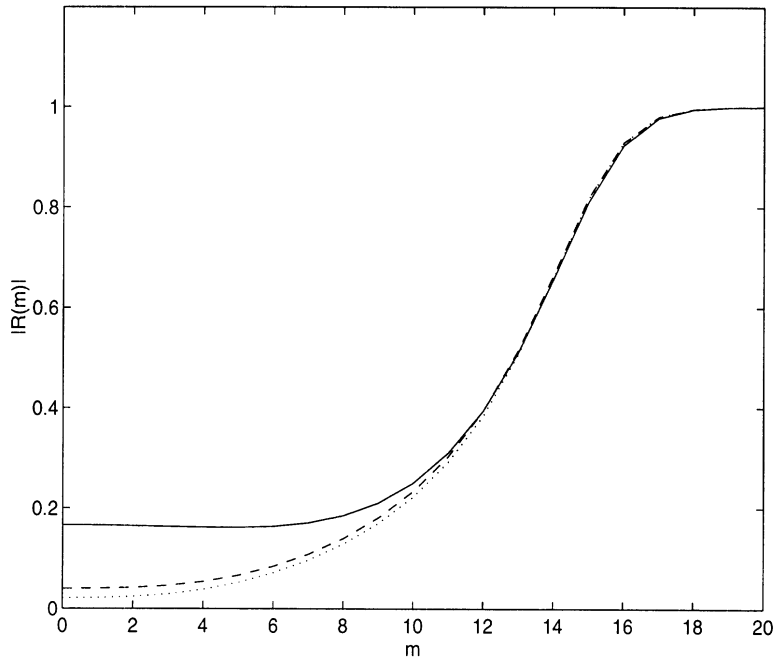

Figure 6: Modal reflection coefficient for a homogeneous isotropic layer at $x_1 = 10 + \pi$ with $\tau = 0.15\lambda_0$: (——) $b_0 = 1 - j$, (— —) $b_0 = 1 - j2$, and $(\cdots)$ $b_0 = 1 - j3$.

Figure 7 shows $|R(m)|$ for various b_0. Apart from the previously encountered overshoots in the $13 < m < 18$ range, the behavior is seen to be somewhere between a first and a second order ABC. We note that as for the material interface of the previous section, the anisotropic layer behaves similarly to the isotropic one for lower orders m but provides improved absorption as the order increases. This is particularly true for the higher values of losses used.

2.3.3 Inhomogeneous Anisotropic Layer

In the case where the anisotropic layer is inhomogeneous with a profile as discussed in Section 2.2.3, the reflection coefficient is (48) with

$$M_m = H^{(2)}_{b_0 m}(b_0\gamma(x_1)) + \Gamma H^{(1)}_{b_0 m}(b_0\gamma(x_1)), \tag{55}$$

$$N_m = \frac{\gamma(x_1)}{x_1}\left[H^{(2)\,\prime}_{b_0 m}(b_0\gamma(x_1)) + \Gamma H^{(1)\,\prime}_{b_0 m}(b_0\gamma(x_1))\right], \tag{56}$$

and

$$\Gamma = -\frac{H^{(2)\,\prime}_{b_0 m}(b_0\gamma(x_2))}{H^{(1)\,\prime}_{b_0 m}(b_0\gamma(x_2))}. \tag{57}$$

The material profile $\gamma(x)$ is given in (47). Figure 8 shows the behavior of $|R(m)|$ as a function of m. As for the material interfaces, an inhomogeneous anisotropic layer provides the best

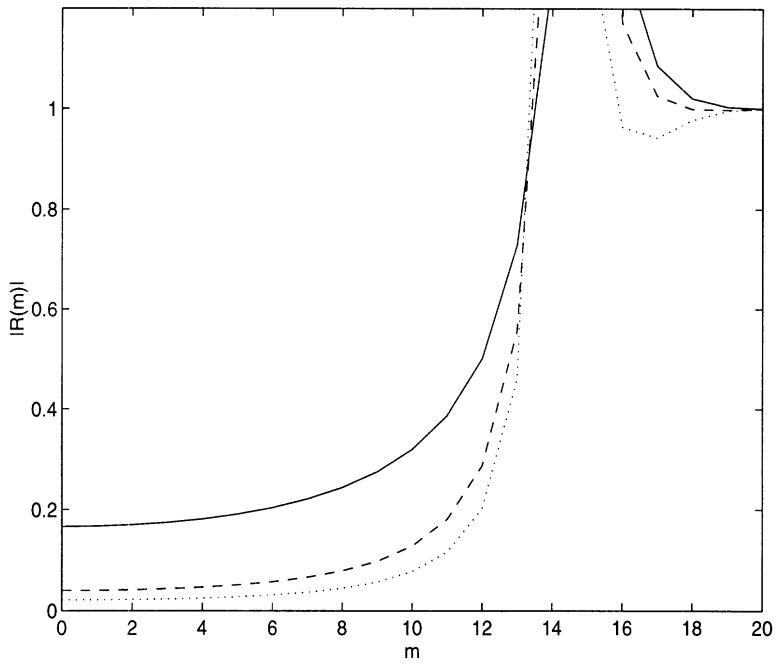

Figure 7: Modal reflection coefficient for a homogeneous anisotropic layer at ρ_1 with $\tau = 0.15\lambda_0$: (——) $b_0 = 1 - j$, (— —) $b_0 = 1 - j2$, and $(\cdots)$ $b_0 = 1 - j3$.

performance overall, especially so when a higher loss is used. Consistent with the previous results, the sharp fluctuations can still be observed.

3 Application: Scattering from a pec cylinder

To better illustrate the performance of the various mesh termination schemes, we now apply them to the problem of scattering from a pec cylinder. The geometry is basically that of Figure 1, save that the arbitrary central body is now specified as a pec circular cylinder of radius $x = x_0 < x_1$ on which impinges an H polarized plane wave incident in the positive x direction. The cylinder is surrounded by an ABC or a material absorber located at $x_1 = x_0 + d$. The scattered field may be written as

$$H_z^s = \sum_{m=-\infty}^{\infty} \left[\tilde{a}_m H_m^{(2)}(k_0\rho) + \tilde{b}_m H_m^{(1)}(k_0\rho)\right] e^{-jm\phi} \tag{58}$$

in the range $\rho_0 \leq \rho \leq \rho_1$ [7,6]. The coefficients $\tilde{b}_m$ take into account reflections from the imperfect absorber. If the absorber is ideal then $\tilde{b}_m$ vanishes and $\tilde{a}_m = a_m$, recovering the exact solution given by

$$a_m = -j^m \frac{J_m'(x_0)}{H_m^{(2)'}(x_0)}. \tag{59}$$

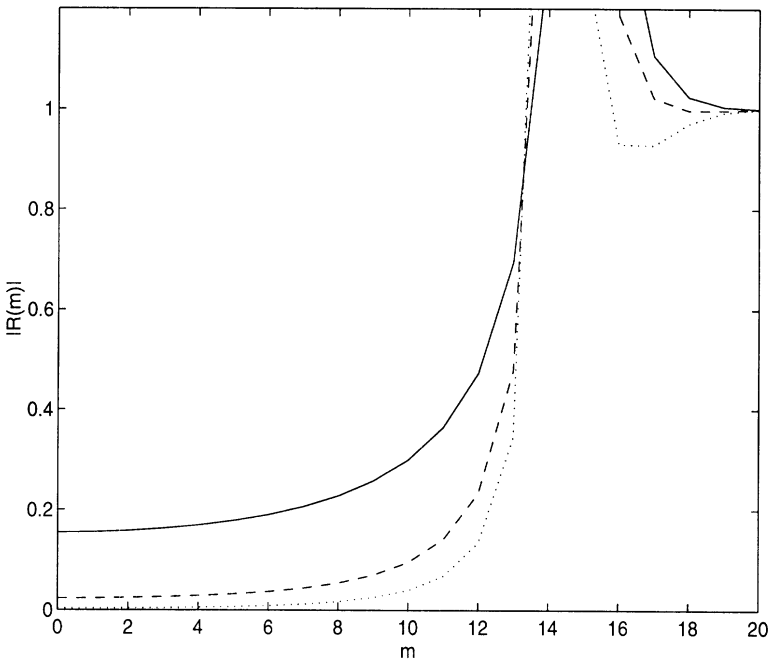

Figure 8: Modal reflection coefficient for a inhomogeneous anisotropic layer at ρ_1 with $\tau = 0.15\lambda_0$: (——) $b_0 = 1 - j$, (— —) $b_0 = 1 - j2$, and $(\cdots)$ $b_0 = 1 - j3$.

The various terminations are easily applied and it can be shown that

$$\tilde{a}_m = a_m \frac{1}{1 + R(m)\frac{H_m^{(1)'}(x_1)}{H_m^{(2)'}(x_1)}} \tag{60}$$

and

$$\tilde{b}_m = R(m)\tilde{a}_m. \tag{61}$$

We confine our attention to a cylinder of radius $x_0 = 10$ with an absorbing termination located at a distance of $d = \lambda_0/2$ such that $x_1 = x_0 + \pi$. Typical results for $|\tilde{a}_m|$ are shown in Figure 9 which compares the exact solution with the ones obtained using the ABCs. We note that the smallest errors are obtained for lower values of m and that the highest error occurs at $m \simeq 10$. Such a presentation is of limited value and we focus instead on the behavior of $|\tilde{b}_m|$ as shown in Figures 10 and 11. This is more useful for comparison purposes as $|\tilde{b}_m|$ ideally goes to zero. Figure 10 compares the performance of the various ABCs with the material interfaces given in Section 2.2. As previously noted, the homogeneous isotropic material follows the poorer first order ABC performance quite well. It is also seen that the homogeneous anisotropic material is between a first and a second order ABC, its performance improving with m relative to the 1st order ABCs. Lastly, as expected, the inhomogeneous anisotropic medium provides the best performance among the material interfaces, being almost as good as a fourth order ABC. Figure 11 presents the same results for layers of

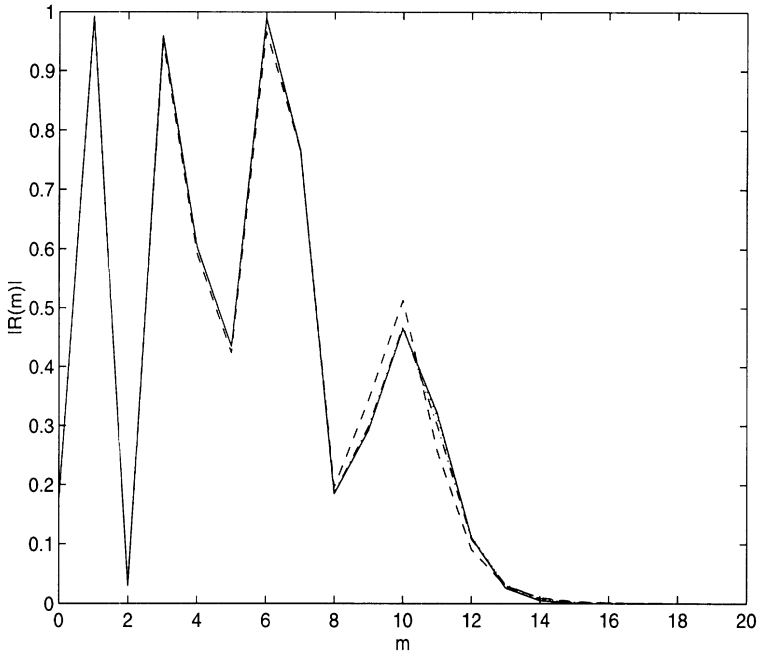

Figure 9: $|\tilde{a}_m|$ with $x_0 = 10$ and $d = \lambda_0/2$: (——) Exact, (— —) 1st order ABC, (– · –) 2nd order ABC, and (· · ·) 4th order ABC.

various thickness, and similar conclusions can be reached. We note that the inhomogeneous anisotropic layer with $b_0 = 1 - j3$ and $\tau = 0.18\lambda_0$ is comparable to a second order ABC.

The effect of these errors is illustrated in Figures 12 and 13, which show the magnitude of the scattered field on the surface of the cylinder for various terminations. From Figure 12, which shows the performance of the ABCs, we observe that the relatively large errors associated with the first order condition lead to spurious oscillations similar to those for an enhanced creeping wave. With the second order condition the agreement is much better, and better still for the fourth order. Figure 13 provides a similar picture for a selection of metal-backed layers. It is interesting to note the similarity between the field for the homogeneous isotropic layer and the poorer first order ABC. Note also the relatively good performance of the inhomogeneous anisotropic layer. One way to quantify the accuracy is to compute the percent RMS value δ of the magnitude of the relative error in the surface scattered field, viz.

$$\delta = 100 \left\{ \frac{1}{M} \sum_{k=1}^{M} \left| 1 - \frac{U^s_{approx}(\rho_0, \phi_k)}{U^s_{exact}(\rho_0, \phi_k)} \right|^2 \right\}^{1/2} \qquad (percent) \tag{62}$$

where M is the number of angles at which the error is computed, U^s_{exact} is the exact scattered field and U^s_{approx} is the scattered field computed using a given termination. For the data that follow, the errors were computed at one degree increments in ϕ_k, and to appreciate the significance of δ, Tables 1 and 2 give the errors computed using the ABCs and the various materials absorbers, respectively.

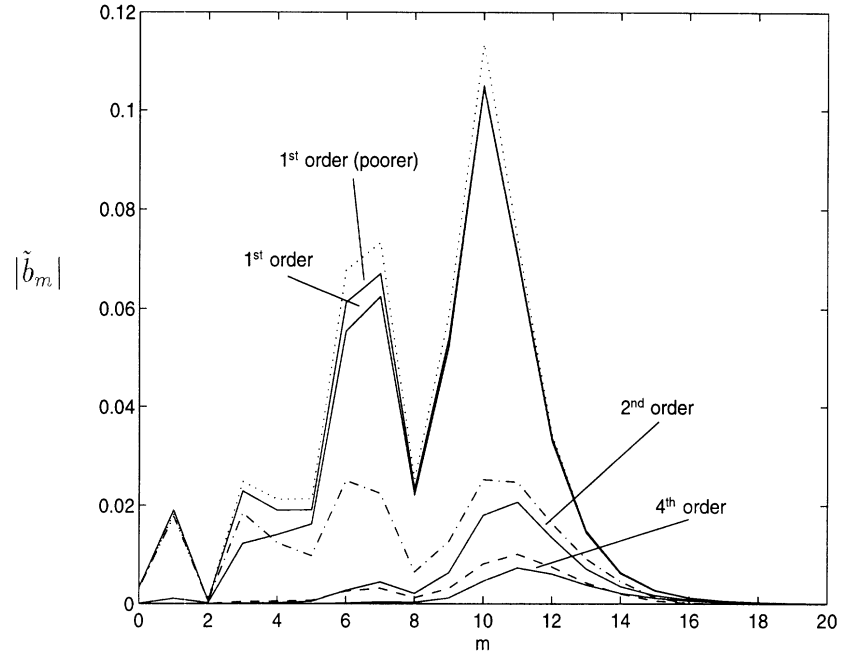

Figure 10: $|\tilde{b}_m|$ for interfaces with $x_0 = 10$ and $d = \lambda_0/2$ and $b_0 = 1 - j3$: (——) ABCs, $(\cdots)$ homogeneous isotropic, (— · —) homogeneous anisotropic, and (— —) inhomogeneous anisotropic.

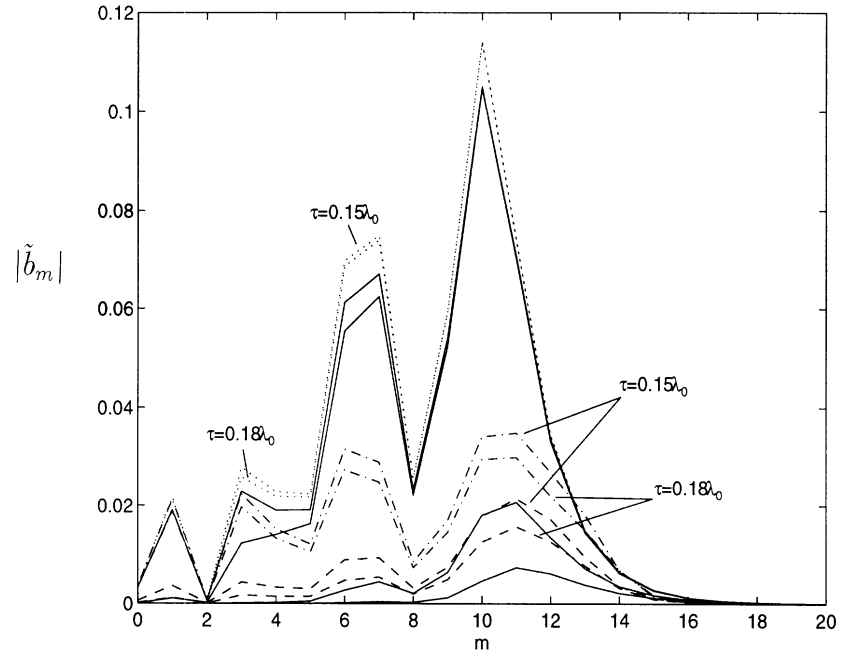

Figure 11: $|\tilde{b}_m|$ for layers with $x_0 = 10$, $d = \lambda_0/2$ and $b_0 = 1 - j3$: (——) ABCs, $(\cdots)$ homogeneous isotropic, (— · —) homogeneous anisotropic, and (— —) inhomogeneous anisotropic.

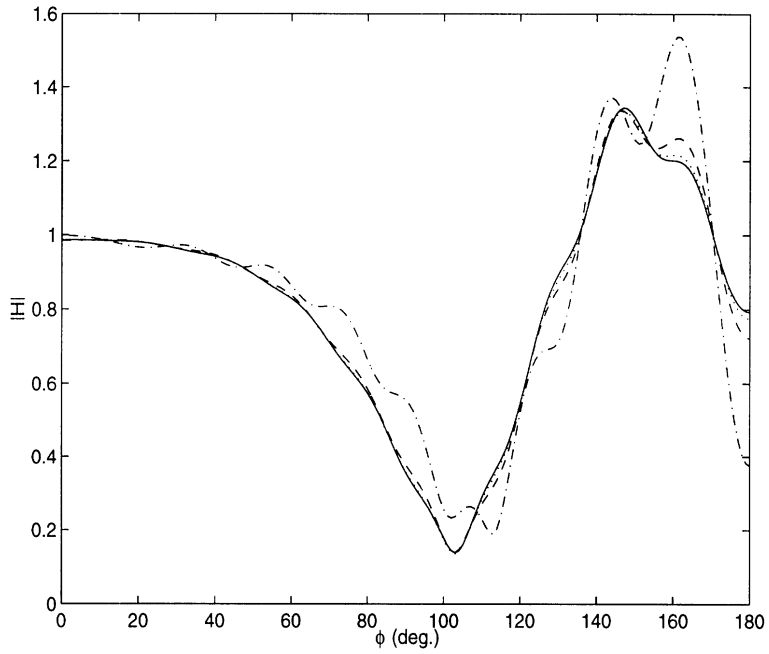

Figure 12: $|H_z^s(x_0)|$ using ABCs when $x_0 = 10$ and $d = 0.5\lambda_0$: (——) exact, (— · —) 1^{st} order ABC (poorer), (— —) 2^{nd} order ABC, and (···) 4^{th} order ABC.

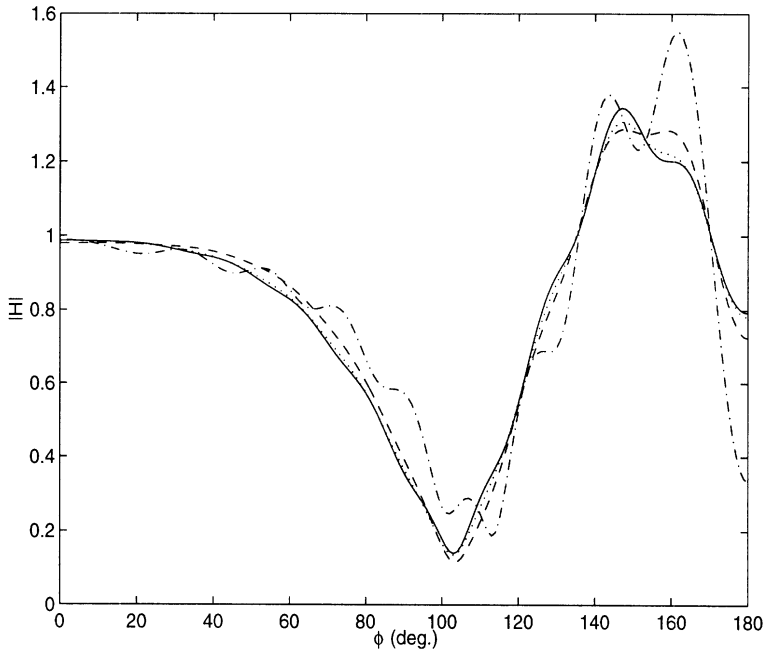

Figure 13: $|H_z^s(x_0)|$ using layers when $x_0 = 10$, $d = \lambda_0/2$, $\tau = 0.18\lambda_0$ and $b_0 = 1 - j3$: (——) exact, (— · —) homogeneous isotropic, (— —) homogeneous anisotropic, and (···) inhomogeneous anisotropic.

ABC	RMS Error
1^{st} order (poorer)	31.80
1^{st} order	31.21
2^{nd} order (poorer)	5.81
2^{nd} order	4.55
4^{th} order (poorer)	2.26
4^{th} order	1.30

Table 1: Percent RMS error of surface field for ABCs

Type	$b_0 = 1 - j$	$b_0 = 1 - j2$	$b_0 = 1 - j3$
Homogeneous Isotropic			
Infinite	35.12	35.80	34.69
$\tau = 0.15\lambda_0$	52.60	37.92	35.05
$\tau = 0.18\lambda_0$	48.99	37.41	34.88
Homogeneous Anisotropic			
Infinite	6.60	8.56	9.24
$\tau = 0.15\lambda_0$	74.90	21.64	12.19
$\tau = 0.18\lambda_0$	54.21	15.76	10.47
Inhomogeneous Anisotropic			
Infinite	1.52	2.02	2.21
$\tau = 0.15\lambda_0$	68.55	14.90	5.21
$\tau = 0.18\lambda_0$	47.94	9.00	3.48

Table 2: Percent RMS error of surface field for material absorbers

Theses errors are presented graphically in Figures 14 to 16 which compare the performance of the terminations in the context of the scattering problem considered. We see, for example, that a second order ABC is bested by an inhomogeneous anisotropic layer of thickness $\tau = 0.18\lambda_0$ and material parameter $b_0 = 1 - j3$.

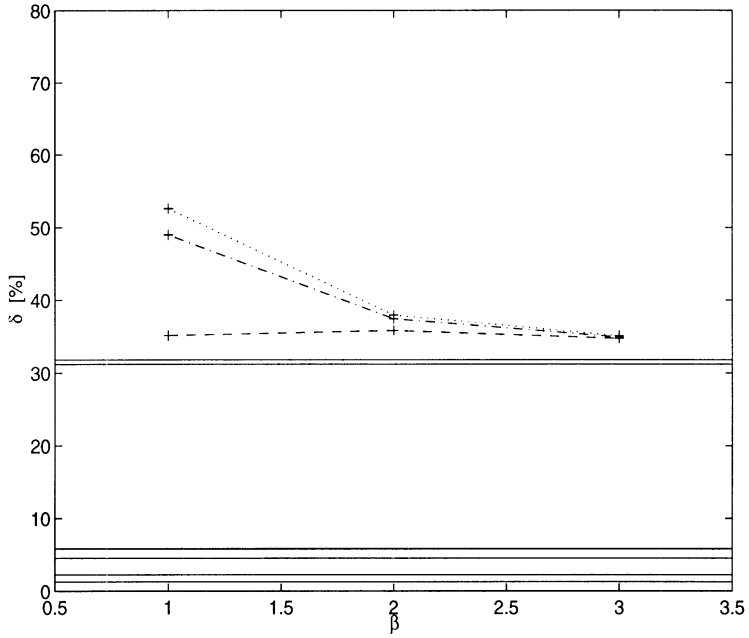

Figure 14: Error δ for ABCs and homogeneous isotropic material with $b_0 = 1 - j\beta$, $x_0 = 10$ and $d = 0.5\lambda_0$: (——) ABCs, $(\cdots)$ layer with $\tau = 0.15\lambda_0$, (— · —) layer with $\tau = 0.18\lambda_0$, and (— —) infinite medium.

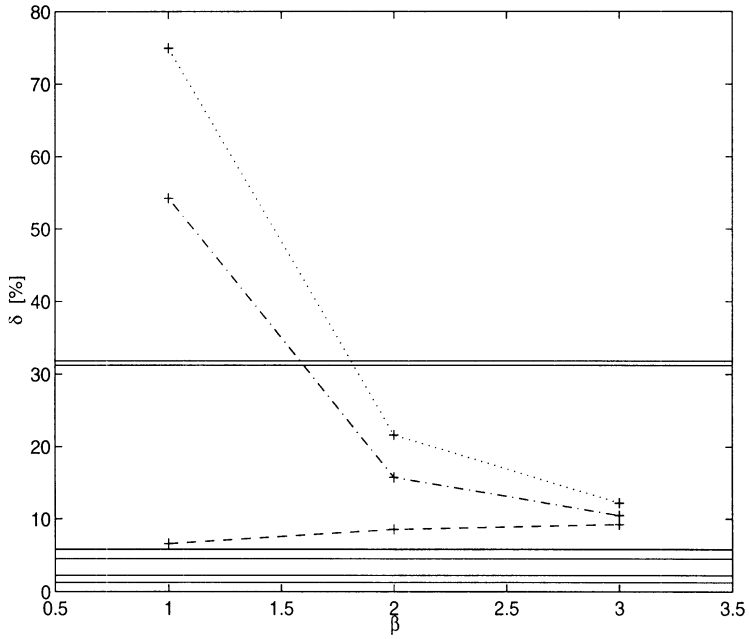

Figure 15: Error δ for ABCs and homogeneous anisotropic material with $b_0 = 1 - j\beta$, $x_0 = 10$ and $d = 0.5\lambda_0$: (——) ABCs, $(\cdots)$ layer with $\tau = 0.15\lambda_0$, (— · —) layer with $\tau = 0.18\lambda_0$, and (— —) infinite medium.

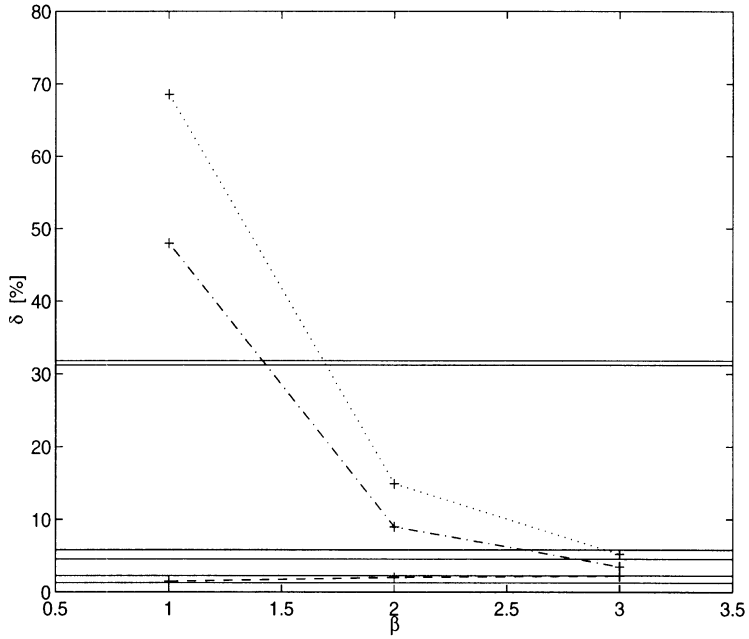

Figure 16: Error δ for ABCs and inhomogeneous anisotropic material with $b_0 = 1 - j\beta$, $x_0 = 10$ and $d = 0.5\lambda_0$: (——) ABCs, $(\cdots)$ layer with $\tau = 0.15\lambda_0$, (— · —) layer with $\tau = 0.18\lambda_0$, and (— —) infinite medium.

A Numerical Evaluation of Hankel Functions

The numerical evaluation of special functions is often a daunting task and the Hankel functions $H_\nu^{(1)}(z)$ and $H_\nu^{(2)}(z)$ prove to be no exception, especially when complex quantities are involved. In the case where both the order ν and the argument z are real, a number of commercially available packages such as *Matlab* are well suited to evaluate these functions. There are also numerous function libraries, most of them written in FORTRAN 77, which provide routines for similar purposes. The number of adequate packages is, however, narrowed if the argument is complex. One of the better libraries is the AMOS function library. It provides a wide range of routines for Bessel related functions valid for real order and complex arguments. The package is easily obtained through Netlib and the interested reader is referred to [8] for additional details. We note here that simply computing the Hankel function from the Bessel and the Neumann functions using, for example,

$$H_\nu^{(2)}(z) = J_\nu(z) - jN_\nu(z) \tag{63}$$

is often numerically inaccurate for some combinations of z and ν and specialized routines to compute Hankel functions such as those provided by the AMOS library become necessary.

When the Hankel functions have complex order and argument, there are no widely available routines, and we must instead resort to using the commercial package *Mathematica*. Once again, as (63) may be numerically inaccurate for some combinations of ν and z, and since *Mathematica* does not provide specific definitions for the Hankel functions, we must instead rely on Bessel functions of the third kind. The formulation used is thus

$$H_\nu^{(1)}(z) = \frac{2}{j\pi} e^{-j\frac{\pi}{2}\nu} K_\nu(jz), \tag{64}$$

$$H_\nu^{(2)}(z) = \frac{2j}{\pi} e^{j\frac{\pi}{2}\nu} K_\nu(-jz). \tag{65}$$

The Wronskians were computed in order to verify the results. An interesting discussion about the evaluation of Hankel function with complex order and argument is given by Paknys [9] and his results were successfully duplicated.

References

[1] T.B.A. Senior and J.L. Volakis, *Approximate Boundary Conditions in Electromagnetics.* Stevenage, UK, IEE Press, 1995.

[2] S.R. Legault and T.B.A. Senior, "Matched planar surfaces and layers," University of Michigan Radiation Laboratory Report No. 929, 1995.

[3] T. Özdemir and J.L. Volakis, "A comparative study of an absorbing boundary condition and an artificial absorber for truncating finite element meshes," *Radio Sci.* **29**, pp. 1255-1263, 1994.

[4] Z.S. Sacks, D.M. Kingsland, R. Lee and J.F. Lee, "A perfectly matched anisotropic absorber for use as an absorbing boundary condition," to appear in *IEEE Trans. Antennas Propagat.*

[5] S. M. Rytov,"Calcul du skin-effect par la méthode des perturbations," *J. Phys. USSR* **2**, pp. 233-242, 1940.

[6] T.B.A. Senior, J.L. Volakis and S.R. Legault, "Higher Order Impedance and Absorbing Boundary Conditions", to appear in *IEEE Trans. Antennas Propagat.*

[7] R. Mittra and O. Ramahi, "Absorbing boundary conditions for the direct solution of partial differential equation," *Progress in Electromagnetics Research*, M.A. Morgan, ed., Newark, Elsevier, pp.133-173, 1990.

[8] D.E. Amos, "ALGORITHM 644, A Portable Package for Bessel Functions of a Complex Argument and Nonnegative Order", *ACM Trans. Math. Software* **12**, pp. 265-273, 1986.

[9] R. Paknys, "Evaluation of Hankel Functions with Complex Argument and Complex Order", *IEEE Trans. Antenn. Propagat.* **40**, pp. 569-578, 1992.